mathematics

MDPI

Article

On the Fractional Dynamics of Kinks in Sine-Gordon Models

Tassos Bountis [1,*], Julia Cantisán [2], Jesús Cuevas-Maraver [3,4], Jorge Eduardo Macías-Díaz [5,6] and Panayotis G. Kevrekidis [7]

1 Department of Mathematics, University of Patras, 26500 Patras, Greece
2 Grupo de Física No Lineal (FQM-280), Departamento de Ciencias Integradas y Centro de Estudios Avanzados en Física, Matemáticas y Computación, Universidad de Huelva, 21071 Huelva, Spain; julia.cantisan@dci.uhu.es
3 Grupo de Física No Lineal (FQM-280), Departamento de Física Aplicada I, Escuela Politécnica Superior, Universidad de Sevilla, C/ Virgen de África, 7, 41011 Sevilla, Spain; jcuevas@us.es
4 Edificio Celestino Mutis, Instituto de Matemáticas de la Universidad de Sevilla (IMUS), Avenida de la Reina Mercedes s/n, 41012 Sevilla, Spain
5 Department of Mathematics and Didactics of Mathematics, School of Digital Technologies, Tallinn University, Narva Rd. 25, 10120 Tallinn, Estonia; jemacias@correo.uaa.mx
6 Departamento de Matemáticas y Física, Universidad Autónoma de Aguascalientes, Avenida Universidad 940, Ciudad Universitaria, Aguascalientes 20131, Mexico
7 Department of Mathematics and Statistics, University of Massachusetts Amherst, Amherst, MA 01003-4515, USA; kevrekid@umass.edu
* Correspondence: bountis@math.upatras.gr

Abstract: In the present work, we explored the dynamics of single kinks, kink–anti-kink pairs and bound states in the prototypical fractional Klein–Gordon example of the sine-Gordon equation. In particular, we modified the order β of the temporal derivative to that of a Caputo fractional type and found that, for $1 < \beta < 2$, this imposes a dissipative dynamical behavior on the coherent structures. We also examined the variation of a fractional Riesz order α on the spatial derivative. Here, depending on whether this order was below or above the harmonic value $\alpha = 2$, we found, respectively, monotonically attracting kinks, or non-monotonic and potentially attracting or repelling kinks, with a saddle equilibrium separating the two. Finally, we also explored the interplay of the two derivatives, when both Caputo temporal and Riesz spatial derivatives are involved.

Keywords: sine-Gordon equation; kinks; breathers; fractional derivatives; Caputo derivative; Riesz derivative

MSC: 35Q51; 35R11

Academic Editors: Efthymia Meletlidou and Jonathan Blackledge

Received: 5 December 2024
Revised: 21 December 2024
Accepted: 9 January 2025
Published: 10 January 2025

Citation: Bountis, T.; Cantisán, J.; Cuevas-Maraver, J.; Macías-Díaz, J.E.; Kevrekidis, P.G. On the Fractional Dynamics of Kinks in Sine-Gordon Models. *Mathematics* **2025**, *13*, 220. https://doi.org/10.3390/math13020220

1. Introduction

The study of physical, chemical and biological applications of fractional calculus has been a theme of growing interest over the past few years. Relevant applications extend from optical media [1,2] to epidemiological models [3], and from biological systems [4] to economics [5]. By now, a diverse and broad range of corresponding models has been summarized in books and associated reviews. Some of them are more topical, such as, e.g., [6], focusing on fractional models of dispersive waves, while others are of more general interest, see, e.g., [7,8].

The field of wave dynamics has been a fertile platform for the investigation of such ideas, as has been demonstrated by the introduction of the fractional Schrödinger equation in optics through the work of [2]. Experimental realizations of related ideas, in the linear regime, have also appeared in the literature, see, e.g., [1]. A wide palette of analytical and

numerical results, linear, as well as nonlinear, continuum, and also (long-range) discrete, were recently reported in [6]. Indeed, such wave phenomena hold considerable promise for further experimental realizations, including the nonlinear regime, given the extensive efforts of many scientists to engineer and control dispersion, which has been spearheaded in recent years by the works of [9,10] (see also [11,12]). Very recently, the first nonlinear waves experiment—to the best of our knowledge—in a spatially fractional dispersive setting was reported in the work of [13]. Such an experiment in the realm of nonlinear optics paves the way for future tailoring of dispersive properties in optics, as well as in other fields and renders, which is especially timely with the consideration of prototypical nonlinear, fractional dispersive partial differential equation models, such as fractional variants of the Korteweg-De Vries equation, the nonlinear Schrödinger equation and the sine-Gordon equation, among others [6].

With that spirit and motivation in mind, in the present work, we build on recent studies of spatially fractional models of the ϕ^4 type in [14] by examining the famous sine-Gordon equation [15] with fractional derivatives in both space and time. While the relevant integer derivative models first appeared in the context of constant negative curvature surfaces [16], the sine-Gordon equation has also often emerged in numerous other subfields of solid state physics, biophysics and beyond. For instance, in its discrete form, it is a widespread model of the dynamics of crystal dislocations [17], while it has also been thoroughly examined in the context of Josephson junction arrays [18] and the dynamics of DNA models, among other areas [19].

More precisely, we consider herein, the modification of the prototypical sine-Gordon model under the effect of spatial Riesz derivatives, which is motivated in part by the possibility to engineer dispersion [9,10,13], as well as the introduction of temporal Caputo derivatives. The latter is also motivated by the earlier work of two of the present authors [20], where suitable discretizations for such models were first introduced.

After setting up the general framework of our model in Section 2, we proceed to examine three distinct scenarios: In Section 3, we vary the order of the temporal (Caputo) derivative, while preserving the sine-Gordon (sG) right hand side. Here, we see, for instance, how kinks slow down in the presence of the Caputo temporal fractional derivatives and appear to exhibit a dissipative effective motion. In Section 4, we return to the temporal second derivative and allow the spatial derivative order to change in the evaluation of the Riesz derivative. An important finding in this setting is the disparity between the case of Riesz exponents above the value for the harmonic case (where there is a stationary kink–antikink bound state with non-monotonic tails) and the exponent below the harmonic, leading to a power law decay, which is, however, always monotonic in this limit. Then, in Section 5, we combine these variations. In each case, we consider first the dynamics of the single kink (the prototypical coherent structure) before exploring multi-kink or bound states thereof in the form of kink–anti-kink or breather initial conditions. In this setting, the above features, when combined, give rise to intriguing kink–anti-kink and breather dynamics, including, e.g., kink–anti-kink annihilation or separation and breathers that produce a kink–anti-kink pair that may or may not decay at long evolution times. Finally, in Section 6, we summarize our findings and discuss some directions for possible future studies.

2. Model Setup

The general problem we study here concerns different types of solutions of the fractional sine-Gordon equation:

$$\frac{\partial^\beta u}{\partial t^\beta} = \frac{\partial^\alpha u}{\partial x^\alpha} - \sin(u). \tag{1}$$

For the integrable case $\alpha = \beta = 2$, the solutions of Equation (1) are well known [15]. To appreciate the effect of fractional derivatives, we consider the following cases of interest:

1. A Caputo derivative of order $\beta \neq 2$ in time but a second derivative in space.
2. A Riesz derivative of order $\alpha \neq 2$ in space but a second derivative in time.
3. The general case, where a a Caputo derivative of order $\beta \neq 2$ in time is combined with a Riesz derivative of order $\alpha \neq 2$ in space.

Our aim in all cases was to explore the dynamics of the single kink, as well as the kink–anti-kink pair (and related structures of particular relevance to the sine-Gordon continuum model [21]) in the presence of fractional derivatives. Our motivation here is analogous to the recent development of [13] within nonlinear optics. If, in any of the diverse settings mentioned in the Introduction (see, e.g., an over-arching summary of the book of [15]), the possibility to experimentally manipulate/engineer dispersion similarly arises, then Equation (1) emerges as the canonical fractional derivative extension thereof.

We consider Caputo derivatives, instead of, e.g., those of Riemann–Liouville type, as, in the former case, the initial conditions are immediately retrieved from the integer derivative case, see, e.g., [7,8] for relevant details. Indeed, one can then specify $u(0,x)$ and $\partial_t u(0,x)$, as is, in general, natural for initial value problems such as the ones specified herein. The algorithm used for numerical integration is `fde_pi12_pc`, which can be found in [22].

3. Caputo Derivative in Time and Laplacian in Space

We start with Case 1 above: preserving the spatial Laplacian and only modifying the time derivative in the form of a variable Caputo exponent.

3.1. Kink Dynamics

First, we examine the most prototypical waveform solution of the model, namely the single kink. We consider, as our Riesz exponent, $\alpha = 2$ and values of the Caputo exponent $\beta < 2$. We also comment on the case with $\beta > 2$ later on. As the initial condition for Equation (1), we consider

$$((u(x,0), \dot{u}(x,0)) = (u_0, \dot{u}_0) = (4 \arctan e^{\gamma_0 x}, -2\gamma_0 v_0 \operatorname{sech}(\gamma_0 x)), \tag{2}$$

where the overdot stands for the partial derivative in time and

$$\gamma_0 = \frac{1}{\sqrt{1 - v_0^2}} \tag{3}$$

represents the Lorentz contraction factor [15].

For $\beta = 2$, the kink propagates at a constant speed $v = v_0$, which we fix to 0.2, as expected from the corresponding exact solution. However, when fractionality is introduced in the equation, and we consider derivative orders $\beta < 2$, the kink velocity *decays in time*. This is shown in Figure 1, where spatio-temporal plots of $u(x,t)$ for $\beta = 2$ and $\beta = 1.9$ are compared. In addition, the left panel of Figure 2 depicts the kink velocity evolution as a function of time. Here, we can clearly observe the dissipative effect of the Caputo derivative. The kink naturally slows down and the velocity eventually tends to zero. Indeed, similar features were first reported for breathers in the time-fractional sine-Gordon equation [20,23], where the oscillations were first shown to be damped for values of $\beta < 2$. It is this parameter setting that we also explore herein.

Remarkably, the velocity of the kink decays exponentially over time after an initial short (transient) interval. This is clearly seen in the left panel of Figure 2, where the

exponential fit is depicted as a black dashed line for $\beta = 1.5$, in excellent agreement with the PDE results. We define, by τ, the characteristic time at which the velocity halves, and we marked it in the figure with an horizontal gray dashed line. In the right panel of Figure 2, we plotted the variation of the inverse of characteristic time with respect to the order of the Caputo derivative. As β approaches the value 2, τ tends to infinity and the inverse tends to zero, as one would expect, based on the absence of dissipation in that limit. In the same panel, we included a logarithmic fit of the following form: $1/\tau = a \cdot \log(b \cdot |\beta - 2| + 1)$, with $a = 0.0581$, $b = 2.6410$ and $r = 0.9998$.

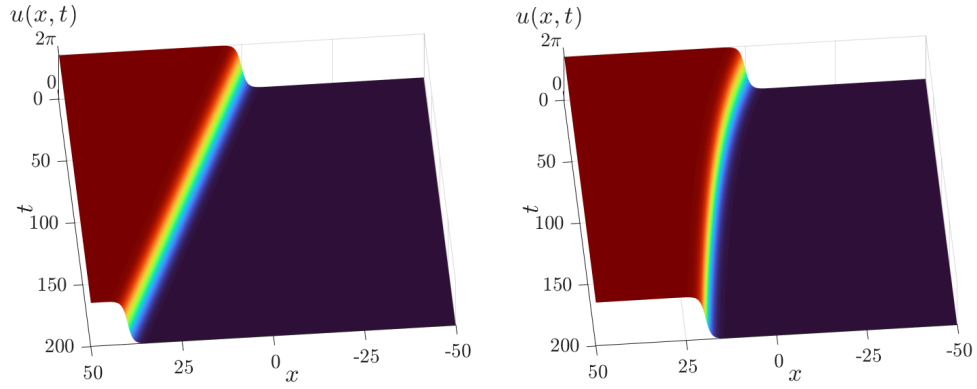

Figure 1. Time evolution of the kink with initial velocity $v_0 = 0.2$ for the ordinary Laplacian ($\alpha = 2$). Panels show $u(x, t)$ and compare the Hamiltonian constant–velocity dynamics of $\beta = 2$ (**left**) and the decelerating dynamics of the Caputo-fractional case of $\beta = 1.9$ (**right**). Notice how the former panel showcases a traveling kink, while, for the latter, the kink trajectory starts "bending", reflecting the kinks' temporal slowdown.

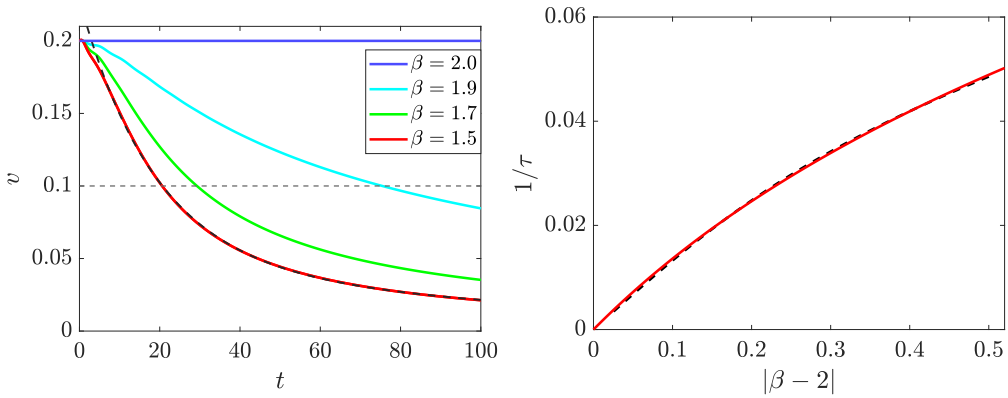

Figure 2. Left panel: Kink velocity decay with the order of the Caputo derivative. For $\beta = 2$, the kink propagated at a constant velocity. The fractionality acts as form of damping, exponentially decreasing the velocity. For $\beta = 1.5$, the exponential fit is represented by a dashed black line. We defined τ as the time for which the velocity halves ($v = 0.1$, also marked here in gray) for each β value. **Right panel**: Inverse of the characteristic time with respect to the order of the Caputo derivative. As β approached 2, the characteristic time tended to infinity (i.e., $1/\tau$ tends to zero) since the kink motion was undamped in that limit. The dotted black line depicts the numerical results and the red solid line is a logarithmic fit.

It is interesting to complement the above results with the case of a kink that is stationary, in part because this is the ultimate fate of the structure in the model bearing a Caputo derivative, but also to compare/contrast the relevant phenomenology with that of the standard (conservative) sine-Gordon case. Thus, when initializing Equation (1) for vanishing velocity $v_0 = 0$, one observes the left panel of Figure 3 for $\beta = 2$ and the right panel for $\beta = 1.9$. In the left panel, we show, in logarithmic scale, the pulse-like derivative of the kink, and we observe that the approximation induced numerically by the

local truncation error leads to the propagation of radiation wakes that move toward the boundary and eventually is reflected from it, returning to the kink and impinging upon it. The orange dominant color in these radiation waves reflects this discretization-induced error for our spatial discretization of spacing of $O(10^{-1})$. Importantly, the radiation is never "washed away" given the Hamiltonian nature of the model. It is relevant to note here that, in this stationary case, had we presented the 3D profile of $u = u(x,t)$, the left and right panels would be indiscernible as the $0 - 2\pi$ scale of such panels would not permit one to distinguish their much smaller scale differences.

On the contrary, the right panel of the figure shows quite a different picture for the case of a Caputo derivative with $\beta = 1.9$. What we see is that the color associated with the radiation wakes drastically changes from orange to yellow and gradually to green and blue, reflecting the dissipative nature of the corresponding derivative and essentially the "annihilation" of the relevant wakes, or, as otherwise stated, the "distilling" of the kink into the appropriate stationary state of the model. That is to say, these computations, both at the dynamical level of the slowing down moving kink, but also at the stationary level of the static kink, reflect the dissipative nature of the effect of the Caputo temporal derivative.

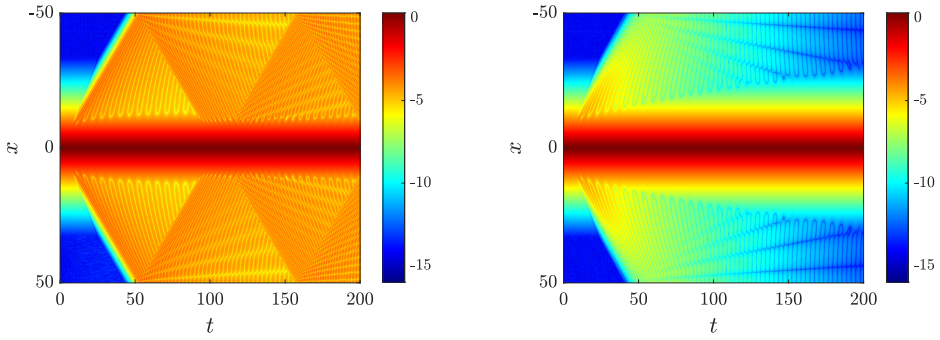

Figure 3. Time evolution of the pulse-like derivative of a stationary kink with weak (numerical scheme-induced) radiation on top of an exact stationary kink solution, which is when fixed ends boundary conditions and ordinary Laplacian ($\alpha = 2$) are considered. Panels show $\log_{10}|\partial_x u(x,t)|$ and distinguish between the radiation-reflecting case of $\beta = 2$ (**left**) and the "radiation-removing" case of $\beta = 1.9$ (**right**). Thus, radiation is "distilled" (eliminated) in the Caputo-fractional case of $\beta = 1.9$, while it hits the boundary and returns in the Hamiltonian ($\beta = 2$) case.

3.2. Kink–Anti-Kink Dynamics

Let us now consider the dynamics of head-on collisions of kink–anti-kink pairs in the Caputo time derivative case with $\beta < 2$. To this end, we assume an initial condition of the form

$$(u_0, \dot{u}_0) = (4[\arctan e^{\gamma_0(x+\delta)} - \arctan e^{\gamma_0(x-\delta)}], -2\gamma_0 v_0[\mathrm{sech}(\gamma_0(x+\delta)) + \mathrm{sech}(\gamma_0(x-\delta))]. \quad (4)$$

If β is slightly smaller than 2, we observe that, if v_0 is above a certain threshold, the dynamics are similar to the $\beta = 2$ case, namely the collision is quasi-elastic, is followed by an inversion of the kink–anti-kink roles and a subsequent deceleration of the kink–anti-kink is similar to that previously observed for the individual kink. Below this threshold velocity v_0, the kink–anti-kink pair collapses to a breather-like structure that decays in time in a form similar to what was observed in [23]. For a value of $\beta = 1.95$, the threshold v_0 is approximately 0.590.

Figure 4 shows, for $\beta = 1.95$, representative examples of these behaviors. More specifically, these simulations suggest that the damped kink–anti-kink interaction dynamics is still subject (as in the standard sG model) to an attractive interaction potential well with finite depth [24].

Contrary to the standard integrable sG case, however, where the dynamics inside this well is conservative, here the dynamics is dissipative, as shown clearly on the left panel of Figure 4. Thus, in order to escape, the kinks need to overcome both each other's attraction and the reduction in their speed due to dissipation. Understanding the energetics and precise dynamics of the corresponding waveforms as a function of β is certainly an intriguing question that needs further exploration.

When β decreases, the critical v_0 increases and, if β is far enough from 2, this critical value is very close to 1, and the kinks progressively widen before they interact at the same time. It is worth mentioning that the critical v_0 also depends on the initial separation 2δ, so that v_0 increases when δ increases. This is clearly due to the individual dissipative effect of the Caputo derivative on each kink prior to their interaction.

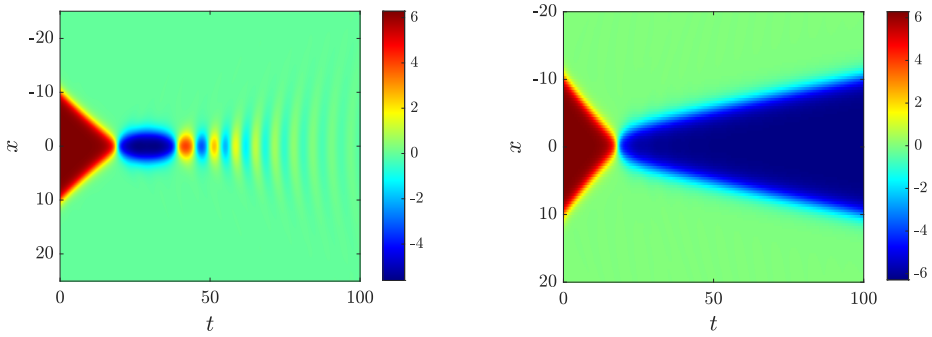

Figure 4. The evolution of a kink–anti-kink pair is initially separated by a distance $2\delta = 20$, and it is launched with an initial velocity v_0, for $\beta = 1.95$ and $\alpha = 2$. The **left** panel shows the generation of a subsequently vanishing breather when $v_0 = 0.55$, whereas the **right** panel corresponds to a quasi-elastic collision occurring when $v_0 = 0.6$. The critical value separating the two regimes is $v_0 \approx 0.590$.

4. Riesz Derivative in Space and Conservative ($\beta = 2$) Dynamics in Time

Having explored the case of varying the order of the time derivative, we now turn to the examination of what happens when the order of the space derivative is varied. In particular, we examine the spatial Riesz derivative order α and the impact of its variation, while we keep the temporal derivative at $\beta = 2$.

4.1. Kink Dynamics

Once again, our first consideration involved the single kink dynamics. Here, we performed a study reminiscent of the recent ϕ^4 model exploration carried out in [14]. In particular, we point out that a single kink has a monotonic spatial profile for $\alpha < 2$, as shown on the left panel of Figure 5, while this changes to a non-monotonic state involving a single crossing of the uniform steady states (of $u = 0$ and $u = 2\pi$) on each side when $\alpha > 2$. This non-monotonicity will be seen below to be connected to the existence of a potential kink–anti-kink (or K-AK) equilibrium in this model. The inset of the figure more clearly highlights the relevant spatial behavior.

On the other hand, in this setting, we not only explored the existence problem, identifying the relevant stationary kink, but we also examined the corresponding linearization problem associated with spectral stability. The relevant eigenvalue problem is based on the ansatz $u(x,t) = u_0(x) + \epsilon e^{\lambda t} w(x)$, where $u_0(x)$ is the spatially stationary configuration (in the context of this subsection the single kink) and leads to the following form:

$$\lambda^2 w = \frac{\partial^\alpha w}{\partial x^\alpha} - \cos(u_0) w. \tag{5}$$

The results of the spectral analysis are shown on the right panel of Figure 5. Here, we see that the mode (in red) sitting at the band edge in the form of a resonance for the standard integrable sine-Gordon case bifurcates from there for $\alpha > 2$ and, indeed, becomes an internal breathing mode of the kink coherent structure. Such internal modes have been of considerable interest in the context of models such as the perturbed sG equation [25]. On the other hand, for the case of $\alpha < 2$, the kink follows an opposite trajectory moving inside of the continuous spectrum. In either case here, this does not affect the spectral stability of the kink, but may affect the outcome of kink collisional interactions, as is well known to occur in the presence of relevant internal modes [26]. Such a topic is outside the scope of the present work and may be of interest in a future study.

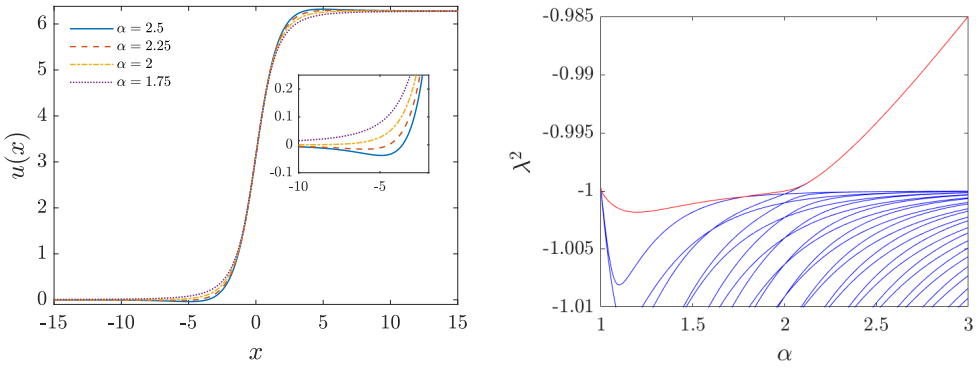

Figure 5. Single-kink Riesz derivative of a fractional order α in space, with $\beta = 2$ in time. The **left** panel shows the stationary kink for four different values of the spatial derivative order α, namely $\alpha = 2.5$, $\alpha = 2.25$ $\alpha = 2$ and $\alpha = 1.75$. Observe the non-monotonic nature of the kink for $\alpha > 2$, while the structure becomes monotonic for $\alpha \leq 2$. The **right** panel shows the (squares of the) lowest non-zero eigenvalues of the kink spectrum as a function of α. The eigenvalue positioned at the band edge $\lambda = \pm i$ in the integrable case of $\alpha = 2$, shown here in red, moves inside the continuous spectrum for $\alpha < 2$, while it becomes an "internal mode" of the kink for $\alpha > 2$. The kink is spectrally stable for all considered values of α.

4.2. Kink–Anti-Kink and Breather Dynamics

The examination of K-AK pairs in the setting of the Riesz spatial derivative is quite interesting in its own right, as manifested in Figure 6. Here, we can see that, for all values of $\alpha > 2$, a K-AK bound state pair exists. Indeed, this pair bifurcates from ∞ as the separation between K and AK diverges for $\alpha \to 2^+$. Such an equilibrium is closely intertwined with the non-monotonic nature of the tail and the existence of the zero crossing within such a tail. It has been well known for some time [27] that the nature of the solitary wave tail is responsible for the force between the solitary waves, as the latter is mediated through the tails. Accordingly, our observation in the previous subsection about the existence of a zero crossing of the kink tail leads to the emergence of a zero-crossing of the force between a kink and an anti-kink. This, in turn, is responsible for the emergence of a K-AK bound state, as illustrated for different values of the Riesz exponent α in Figure 6.

When analyzing the stability of this configuration, as shown in the right panel of Figure 6, we find that the relevant state is generically unstable. The corresponding unstable eigenmode has an eigenvalue which tends to 0 as the K-AK separation tends to ∞, restoring the stability of isolated kinks in the limit of $\alpha \to 2^+$. At the same time, exploring the eigenvector associated with the instability, we see that it is related to the K-AK out-of-phase motion. At the same time, the very fact that this is an unstable fixed point of the PDE strongly suggests that this K-AK stationary configuration represents an energetic maximum (i.e., a saddle point) in this Hamiltonian system.

In turn, this has implications for the dynamics shown in Figure 7. Here, kinks with separation lower than a critical value are expected to collapse into each other due to their pairwise attraction. On the other hand, kinks with separations larger than this value are expected to separate indefinitely due to their repulsion (with the force changing from attractive to repulsive at this critical point). We selected two configurations (for a fixed amplitude coincident with the amplitude of the equilibrium K-AK state) that were parametrized by the inverse width of the configuration. The red dashed line represents a configuration where K and AK have a separation larger that the (equilibrium) critical one, while the black dash-dotted line pertains to a smaller separation. Indeed, the latter are shown at the bottom of the left panel to be indefinitely bound to each other, while the former configuration with the structures, being past the energy landscape's saddle point, can be seen to lead to indefinite separation of the kinks, which is in line with our theoretical expectation.

Lastly, in the context of the Riesz derivative variation, we explored the dynamics of breather configurations (as a variant of the K-AK structure). One of the consequences that can be derived from the bottom left panel of Figure 7 is that, indeed, breathers exist for the model with $\beta = 2$ and $\alpha \neq 2$. Although some numerical experiments were performed in [28], they were not directly computed as periodic orbits. Here, we performed such a computation using Fourier-space techniques similar to those developed in [29].

In particular, we show, in Figure 8, the profile of breathers in two cases, one with $\alpha < 2$ and another with $\alpha > 2$, for the frequency $\omega = 0.8$. In this setting, the second and subsequent harmonics of the frequency lie within the continuous spectrum. As can be deduced from the figure (and the insets, featuring the breather tails, as well as their stability), there were no qualitative differences between the two cases. In addition, they featured small wings, as expected because of the breaking of the integrability of the sine-Gordon equation and the resonance of the breather's n-th harmonic frequency with the continuous spectrum when the Laplacian is fractional.

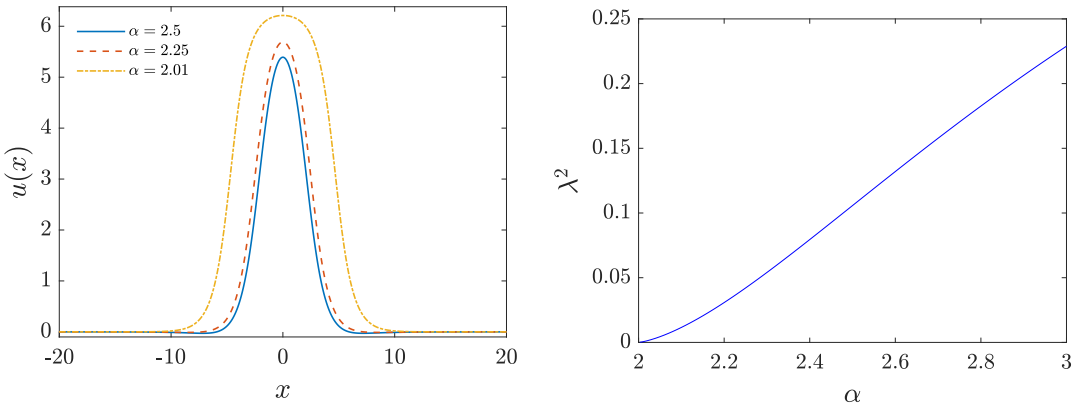

Figure 6. Left panel: kink–anti-kink stationary configuration for a Riesz derivative of a fractional order α in space. The kinks are pinned symmetrically about $x = 0$ and separated by a distance that depends on α. Indeed, a bound state exists $\forall \alpha > 2$. Three different values of α were considered, namely $\alpha = 2.5$, $\alpha = 2.25$ and $\alpha = 2.01$. It can be seen that the distance between the kink and the anti-kink of the bound state *diverges* as the fractional order α approaches the limit $\alpha \to 2^+$. **Right panel**: The eigenvalue pertaining to this kink–anti-kink bound state. We can see that this state is spectrally unstable $\forall \alpha > 2$, and, with the relevant eigenvalue becoming larger, the larger the deviation of α is from its threshold at $\alpha = 2$.

As a consequence, the breather is actually a so-called *nanopteron*, as typically occurs in continuous models with finite domains [15]. Because of the resonances with the linear modes, such models are connected with complex bifurcation diagrams (see [30] for a

relevant example). As a consequence, in the examples shown in Figure 8, we have selected a couple of cases where the breather appeared to be stable in the finite domain computation provided herein. It is relevant to mention that, in order to assess the spectral stability of the breather, standard Floquet multiplier methods were employed based on the eigenvalues of the monodromy matrix, as discussed in, e.g., [31].

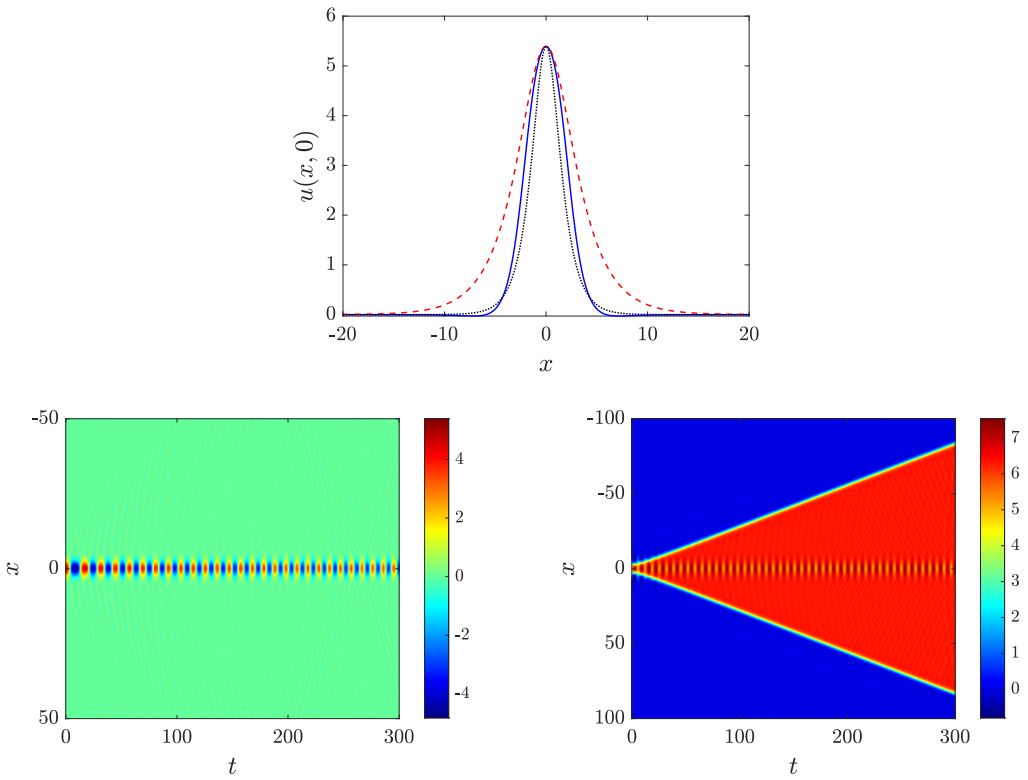

Figure 7. Dynamics of the kink–anti-kink bound state for a fractional order $\alpha = 2.5$ (typical of $\alpha > 2$). In the **top** panel, the blue solid curve represents the equilibrium configuration for $\alpha = 2.5$. The red dashed line corresponds to the initial condition $u(x,0) = A\,\mathrm{sech}(0.4x)$ (with $A \approx 5.3719$ being the maximum amplitude of the K-AK bound state), reflecting a "wider" configuration, while the black dash-dotted line corresponds to the initial condition $u(x,0) = A\,\mathrm{sech}(0.8x)$, pertaining to a "narrower" initial condition. The latter can be seen in the **bottom left** panel to lead the kink and the anti-kink attracting each other and colliding indefinitely forming a breathing state (while emitting radiation). The widening K-AK initial state, on the other hand, lying "outside" of the energy maximum, yields a space–time evolution associated with an indefinite separation of the kink and the anti-kink (see **bottom right** panel).

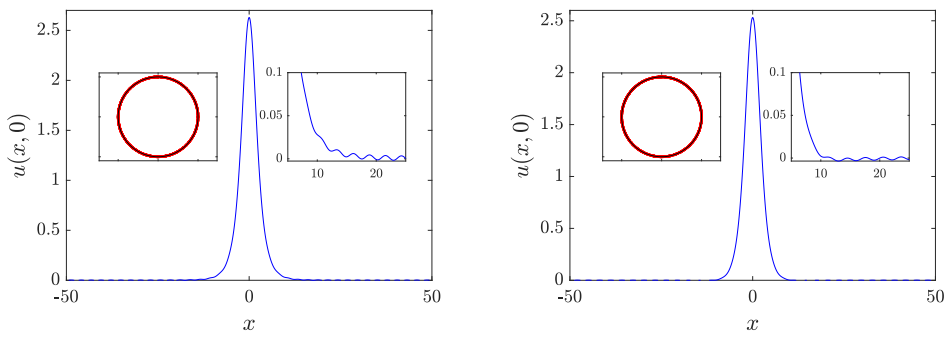

Figure 8. Breathers with $\beta = 2$ and $\alpha = 1.85$ (**left**) and $\beta = 2.15$ (**right**). Their frequency is $\omega = 0.8$ and their domain is $[-50, 50]$. The right inserts in each figure show a zoom on the breather wings, while the left inserts present the Floquet multipliers spectrum.

5. A Caputo Derivative of Order $\beta \neq 2$ and a Riesz Derivative of Order $\alpha \neq 2$

Before discussing our results regarding the dynamics of kinks in this case, it is relevant to remark that, as demonstrated in the Appendix A, the stability spectrum of stationary kinks for any value of β is exactly the same as for $\beta = 2$. The relevant findings indeed apply to the results of Section 3, yet we mention this feature here as it is also true for all values of α. This suggests the intriguing feature that, for $\beta < 2$, while the kink has a spectrum lying on the imaginary axis (i.e., with $\lambda^2 < 0$), the corresponding temporal eigenfunction is responsible for its decay.

5.1. Kink Dynamics

Similarly to the case of $\alpha = 2$, we considered here the dynamics of kinks with an initial velocity v_0 when $\beta < 2$ is varied. To this aim, we took, as an initial condition, a perturbed static kink $u_{\text{kink}}(x)$ of the following form:

$$(u_0, \dot{u}_0) = (u_{\text{kink}}(x), v_0 \partial_x u_{\text{kink}}(x)). \tag{6}$$

This choice of initial conditions was motivated by the difficulty of applying a Lorentz boost to the numerical function $u_{\text{kink}}(x)$ (for values of $\beta \neq 2$).

As can be seen in Figure 9, the dynamics of the kink was almost independent of the value of α and was predominantly dictated by the decay imposed by the presence of the Caputo derivative. Notice, for example, the decay for $\beta = 1.7$, for which we present here for the cases of $\alpha = 1.7$ (solid green line) and $\alpha = 2.5$ (dotted green line). The curves are nearly identical. Consequently, the dynamics for $\alpha \neq 2$ was quite similar as for $\alpha = 2$. The only remarkable difference is the existence of oscillations in the velocity for $\beta = 2$, which is somewhat artificial and is caused by the fact that Equation (6) is not consonant with the Lorentz boost, which can be applied (cf. Equations (2) and (3)) in the latter case, giving rise to a traveling solution.

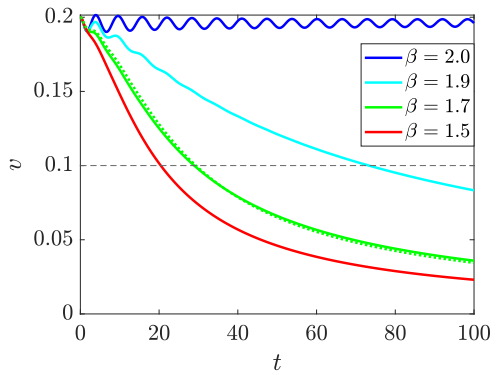

Figure 9. Kink velocity decay with time for different values of the order of the Caputo derivative for $\alpha = 1.7$. We have also included a dotted line for the case $\beta = 1.7$ with a different value of α, which is $\alpha = 2.5$ here for comparison. It can be seen that the value of α barely affects the velocity decay. The initial velocity in all cases was $v_0 = 2$.

5.2. Kink–Anti-Kink Dynamics

In this section, we consider the Riesz derivative and Caputo derivative combined to further study the K-AK pair. First of all, we performed a study similar to the case with $\alpha = 2$, monitoring the dynamics of collisions between kinks and anti-kinks, which were separated at a distance of 2δ. To this end, we took an initial condition of the form

$$(u_0, \dot{u}_0) = (u_{\text{kink}}(x+\delta) + (2\pi - u_{\text{kink}}(x-\delta)), v_0[\partial_x u_{\text{kink}}(x+\delta)) + \partial_x u_{\text{kink}}(x-\delta))]), \tag{7}$$

with $u_{\text{kink}}(x)$ being the stationary kink solution for such a value of α. The observed evolution is qualitatively similar to that of Figure 4; for that reason, no additional figures were included. It must be noticed that, as expected, the critical initial velocity depends on both α and β so that, for a fixed β, the critical v_0 increases when α decreases.

An additional dynamical scenario that we considered involves the evolution of the K-AK pairs in a similar fashion to what was captured in Figure 7, i.e., two localized configurations were considered, one narrower and another one wider than the stationary (and unstable) K-AK pair, initializing the system with a symmetric and stationary such pair. As can be seen in Figure 10, where the same initial condition was taken, for $\beta < 2$, the dynamics were similar to the $\beta = 2$ case, including a dissipative evolution due to the role of the Caputo time-derivative. That is, the generated breather for narrow initial conditions had a vanishing amplitude, whereas the wide initial condition led to an increasing separation (but decelerated in time) for the K-AK pair.

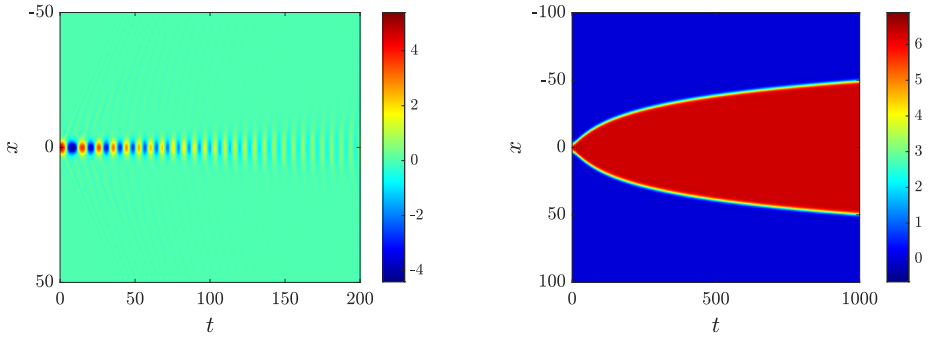

Figure 10. Dynamics of the kink–anti-kink bound state for a fractional order $\alpha = 2.5$ and $\beta < 2$ in a similar fashion to Figure 7. The left panel shows the outcome for $\beta = 1.99$ and an initial condition $u(x,0) = A\,\text{sech}(0.8x)$ (with $A \approx 5.3719$), resulting in a breather whose oscillation decays over time. The right panel corresponds to $\beta = 1.9$ and a "wider" initial condition $u(x,0) = A\,\text{sech}(0.4x)$, leading to a kink and anti-kink whose separation increases in time but in a decelerated fashion.

Finally, we included, as shown in this section, the dynamics of breathers. This aspect involves revisiting, for longer time evolutions, the results of [20] in order to determine the asymptotic fate of such configurations. To that purpose, we considered the initial conditions even in time, namely $u(x,0) = \phi_{\text{br}}(x,0)$

$$\phi(x,0) = 4\arctan\left(\frac{\sqrt{1-\omega^2}}{\omega\cosh(\sqrt{1-\omega^2}x)}\right), \tag{8}$$

and $\dot{u}(x,0) = 0$. For the values of $\beta < 2$, the oscillations of the breather decayed with time. For $u(0,t)$, we fit the maxima and minima to an exponential of the type ae^{-bt}, and we considered the characteristic decay time denoted by $\tau = 1/b$.

As shown in Figure 11, we plotted τ for different values of the Riesz derivative order, fixing the Caputo derivative order to $\beta = 1.99$ and $\beta = 1.9$. The Caputo derivative causes the breather oscillations to decay, as we have previously commented. In this scenario, the Riesz derivative modifies the duration of the transient oscillations, with the oscillations decaying more slowly for higher values of α (for a given β). Notice the difference in the scale of the vertical axis caused by the difference in the values of the Caputo derivative order. The effect of the Riesz derivative was more dramatic for values of β closer to 2. Also, as is transparent already from earlier sections, for a given α, the decay time was higher the closer β was to 2. For values of β much smaller than the ones considered here, oscillations were more rapidly damped and τ was less straightforward to estimate.

Finally, it is interesting to consider here a connection with the earlier work of [20], where a different realization of the breather solution was brought to bear. In particular, in that case, an odd in time initial condition $u(x,0) = 0$ and

$$\dot{u}(x,0) = 4\sqrt{1-\omega^2} \cdot \text{sech}\left(x\sqrt{1-\omega^2}\right) \tag{9}$$

was considered. Remarkably, what was found there was that the system settles in a new transient state, i.e., the end result of the simulation was fundamentally different than the previous decaying state and led to the formation of a K-AK pair. Indeed, in some cases, the latter state appeared in the simulations of [20] as permanent; however, this was the case due to the time horizon of the simulations considered. As shown in Figure 12, to better understand this transient state, we show $u(x,t)$ when the initial condition $u(x,0) = 0$ was considered. Notice that this transient occurs for a small enough value of the breather frequency ω.

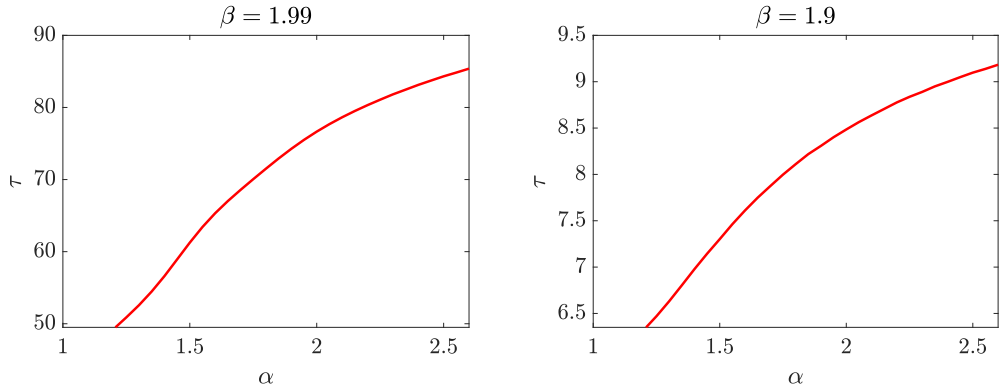

Figure 11. Plots of the characteristic decay time τ for $\beta = 1.99$ (**left panel**) and $\beta = 1.9$ (**right panel**), and different values of the Riesz derivative order α. Here, we consider $\omega = 0.5$.

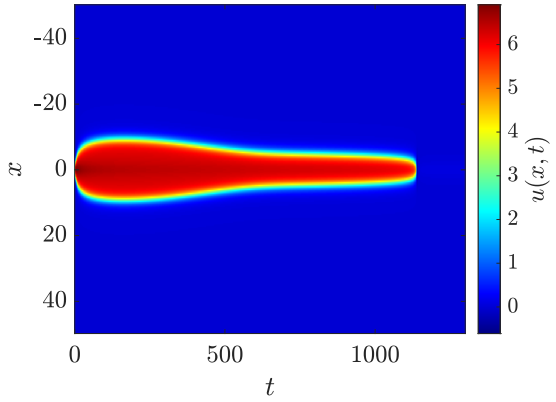

Figure 12. Evolution of $u(x,t)$ for $\beta = 1.4$, $\alpha = 1.8$ and $u_0 = 0$.

Let us study now, in more detail, this transient bound state. To this end, we consider variations of β and study its time duration, which we name T, to avoid confusion with τ, which was considered previously for the damping of the kink velocity. For values of β very close to 2, the behavior of the system is very similar to the non-fractional case. However, for smaller values of β, like $\beta = 1.4$, this transient state is observed for a wide range of values of α. As shown in Figure 13, we show how the duration of the transient bound state depends on the value of the Riesz derivative for $\beta = 1.4$. We observed that, as α approached 2, T increased exponentially. Hence, the relevant state may, depending on the combination of α and β, become extremely long-lived, yet it always has a finite lifetime.

For values of $\alpha \geq 2$ and $1 < \beta < 2$, this bound state is no longer transient, meaning that the system remains in this state. As shown in the right panel of Figure 13, a simulation with a large final time ($t_f = 20 \cdot 10^3$) is shown for $\alpha = 2.01$. In fact, the kink and anti-kink emerging from the breather separate to sufficiently large distances (larger than the equilibrium separation for this α) repelled each other. Because of the periodic boundary conditions that naturally stem from the Riesz derivative and the long-range (power-law) nature of the spatial fractional derivative, each member of the pair experiences two repulsive forces, one from its front and another one from its back, so that they equilibrate at $x = \pm L/4$, with $L = 100$ being the domain length in our case, and, consequently, the kink/anti-kink eventually stopped at that point. We have checked this fact by varying many parameters, such as the initial frequency of the breather, values of $\alpha > 2$ or $\beta < 2$ or domain lengths, all resulting in the same outcome. This settling of the kinks at $x = \pm L/4$ was also observed in the above-mentioned case of kink–anti-kink interactions and the dynamics of unstable K-AK bound states.

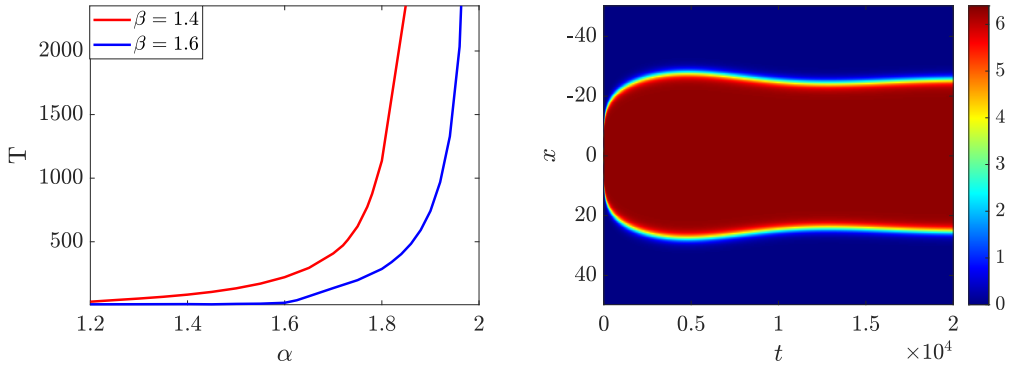

Figure 13. Left panel: Duration of the transient bound state dependence on the value of the Riesz derivative for $\beta = 1.4$ (red line) and $\beta = 1.6$ (blue line). **Right panel**: Bound state for $\beta = 1.7$ and $\alpha = 2.01$. As $\alpha \geq 2$, this state was no longer transient.

6. Conclusions and Future Challenges

In the present work, we explored the fractional dispersive dynamics of the sine-Gordon equation. We achieved this by considering three independent scenarios. In the first one, we imposed a Caputo temporal derivative, while preserving the spatial part of the model. In the second one, we fixed the temporal second derivative and explored the role of variation of the spatial Riesz derivative away from the Laplacian limit. Finally, having understood the role of the previous two variations, we combined them in the final part of our study. In each one of these cases, we explored both the dynamics of a single coherent structure and those of a pair (or a bound state) of such coherent structures.

Our findings clearly showcase some common conclusion paths. The role of the Caputo derivative is to induce dissipative effects in the case where $\beta < 2$. This leads to the slowdown and eventual stopping of a kink, and it may be responsible for the trapping and eventual elimination of a kink–anti-kink pair if the latter does not have sufficient kinetic energy. The presence of a Riesz derivative seems to maintain an attractive kink–anti-kink interaction (through the power-law tails of the still monotonic structures) for $\alpha < 2$. On the other hand, it creates the potential for long-range repulsion through the inter-atomic force for $\alpha > 2$. In the latter case, a saddle equilibrium emerges and the kink acquires non-monotonic tails. The kink–anti-kink interaction, then, evolves in this more complex effective energy landscape, featuring attraction at short and repulsion at long distances. Finally, the phenomenology of both the Caputo temporal and the Riesz spatial derivative together showcase both effects, leading again to decay to stationarity, albeit faster for smaller β and larger α.

Naturally, there exist numerous further directions for future study. On the one hand, while models of the Klein–Gordon type are extremely useful for building intuition (lacking the complexity of phase degrees of freedom), it would be especially instructive to extend considerations to, arguably, the most widespread dispersive nonlinear PDE model, namely the nonlinear Schrödinger equation (see, e.g., [32,33]. In that case, we expect some notable differences, such as the fact that dark soliton bound state pairs may actually feature stable waveforms rather than unstable ones (as seen here) in the presence of Riesz spatial derivatives. On the other hand, there have been numerous intriguing proposals for manipulating dispersion in nonlinear optics [9,11]. Potentially, adapting such proposals to the settings considered herein would be especially meaningful. The very recent experiment of [13], albeit in the bright soliton setting, may pave the wave for a significant surge of activity in this direction. On a related vein, seeking a deeper understanding of the temporally differentiated scenario and its dissipation, through a variational or similar description, would also be of particular interest. These are among the many novel directions (including also higher dimensional settings and the interplay therein) meriting further investigation.

Author Contributions: Conceptualization, T.B. and P.G.K.; methodology, T.B. and P.G.K.; software, J.C.-M. and J.C.; validation, T.B., P.G.K., J.C. and J.E.M.-D.; formal analysis, P.G.K. and T.B.; investigation, P.G.K., J.C. and J.C.-M.; data curation, J.C.-M.; writing—original draft preparation, P.G.K. and T.B.; writing—review and editing, T.B., P.G.K., J.C. and J.E.M.-D.; visualization, J.E.M.-D.; supervision, T.B. and P.G.K.; project administration, T.B. and P.G.K.; funding acquisition, see below. All authors have read and agreed to the published version of the manuscript.

Funding: J.E.M.-D.: The present work reports on a set of final results of the research project "Conservative methods for fractional hyperbolic systems: analysis and applications", which was funded by the National Council for Science and Technology of Mexico (CONACYT) through grant A1-S-45928. This material is based upon work supported by the U.S. National Science Foundation under the awards PHY-2110030, PHY-2408988 and DMS-2204702 (PGK). J.C.-M. acknowledges support from the EU (FEDER program 2014–2020) through MCIN/AEI/10.13039/501100011033 (under the projects PID2020-112620GB-I00 and PID2022-143120OB-I00). J.C. acknowledges that this work has been supported by the Spanish State Research Agency (AEI) and the European Regional Development Fund (ERDF, EU) under project PID2023-148160NB-I00 (MCIN/AEI/10.13039/501100011033).

Data Availability Statement: All data obtained during the research performed in this paper can be obtained from one of the authors of this paper, Jesus Cuevas-Maraver at jcuevas@us.es.

Conflicts of Interest: The authors declare no conflicts of interest.

Appendix A. Stability of Static Kinks

We considered the case when the Caputo derivative in time is combined with the Riesz derivative in space. We will show that the stability of static kinks is independent of the order of the Caputo derivative.

To this aim, let us introduce a perturbation $w(x,t)$ to the static kink given by $u_0(x)$, that is, $u(x,t) = u_0 + \varepsilon w(x,t)$ is introduced in the fractional sine-Gordon equation. Consequently, the perturbation $w(x,t)$ fulfills the following:

$$\frac{\partial^\beta w}{\partial t^\beta} = \left[\frac{\partial^\alpha}{\partial x^\alpha} - \cos(u_0(x))\right] w. \tag{A1}$$

This equation can be solved by separation of variables

$$w(x,t) = E_\beta(\lambda^2 t) v(x), \tag{A2}$$

with $E_\beta(z)$ being the Mittag-Leffler function defined as

$$E_\beta(z) = \sum_{k=0}^{\infty} \frac{z^k}{\Gamma(\beta k + 1)}, \quad z \in \mathbb{C}, \tag{A3}$$

with Γ being Euler's gamma function $\Gamma(x) = \int_0^\infty t^{x-1} e^{-t} dt$. The Mittag–Leffler function has the property that [34]

$$\frac{\partial^\beta E_\beta(\lambda^2 t)}{\partial t^\beta} = \lambda^2 E_\beta(\lambda^2 t) \tag{A4}$$

Thus, the equation for $v(x)$ reads as

$$\lambda^2 v = \left[\frac{\partial^\alpha}{\partial x^\alpha} - \cos(u_0(x)) \right] v, \tag{A5}$$

which is the same equation that one must solve for the stability analysis of the static kink in the case of second derivative in time, except for the time dependence of $w(x,t)$, which is different. However, $E_\beta(\lambda^2 t)$ has a monotonically decreasing dependence (if $0 < \beta < 1$), or a damped oscillatory dependence (if $1 < \beta < 2$), when $\lambda^2 < 0$ and a monotonically (exponential) increase when $\lambda^2 > 0$; the latter property is easily determined by inspecting the definition of the Mittag–Leffler function. Thus, the spectral picture is analogous to the case of $\beta = 2$, with the latter bearing a time dependence $\exp(\lambda t)$. In fact, $E_1(z) = \exp(z)$ and $E_2(z) = \cosh(z)$.

References

1. Malomed, B.A. Optical Solitons and Vortices in Fractional Media: A Mini-Review of Recent Results. *Photonics* **2021**, *8*, 353. [CrossRef]
2. Longhi, S. Fractional schrödinger equation in optics. *Opt. Lett.* **2015**, *40*, 1117–1120. [CrossRef] [PubMed]
3. Qureshi, S. Real life application of caputo fractional derivative for measles epidemiological autonomous dynamical system. *Chaos Solitons Fractals* **2020**, *134*, 109744. [CrossRef]
4. Ionescu, C.; Lopes, A.; Copot, D.; Machado, J.A.T.; Bates, J.H.T. The role of fractional calculus in modeling biological phenomena: A review. *Commun. Nonlinear Sci. Numer. Simul.* **2017**, *51*, 141–159. [CrossRef]
5. Ming, H.; Wang, J.; Fečkan, M. The application of fractional calculus in Chinese economic growth models. *Mathematics* **2019**, *7*, 665. [CrossRef]
6. Kevrekidis, P.; Cuevas-Maraver, J. *Fractional Dispersive Models and Applications*; Springer: Berlin/Heidelberg, Germany, 2024.
7. Podlubny, I. *Fractional Differential Equations: An Introduction to Fractional Derivatives, Fractional Differential Equations, to Methods of Their Solution and Some of Their Applications*; Elsevier: Amsterdam, The Netherlands, 1998; Volume 1998.
8. Samko, S.; Kilbas, A.A.; Marichev, O. *Fractional Integrals and Derivatives—Theory and Applications*; Gordon and Breach: Amsterdam, The Netherlands, 1993.
9. Blanco-Redondo, A.; de Sterke, C.M.; Sipe, J.; Krauss, T.F.; Eggleton, B.J.; Husko, C. Pure-quartic solitons. *Nat. Commun.* **2016**, *7*, 10427. [CrossRef]
10. Runge, A.F.J.; Hudson, D.D.; Tam, K.K.K.; de Sterke, C.M.; Blanco-Redondo, A. The pure-quartic soliton laser. *Nat. Photonics* **2020**, *14*, 492–497. [CrossRef]
11. Tam, K.K.K.; Alexander, T.J.; Blanco-Redondo, A.; de Sterke, C.M. Stationary and dynamical properties of pure-quartic solitons. *Opt. Lett.* **2019**, *44*, 3306–3309. [CrossRef] [PubMed]
12. Tam, K.K.K.; Alexander, T.J.; Blanco-Redondo, A.; de Sterke, C.M. Generalized dispersion Kerr solitons. *Phys. Rev. A* **2020**, *101*, 043822. [CrossRef]
13. Hoang, V.T.; Widjaja, J.; Qiang, Y.L.; Liu, M.; Alexander, T.J.; Runge, A.F.J.; de Sterke, C.M. Observation of fractional evolution in nonlinear optics. *arXiv* **2024**, arXiv:2410.23671.
14. Decker, R.J.; Demirkaya, A.; Alexander, T.J.; Tsolias, G.A.; Kevrekidis, P.G. Fractional solitons: A homotopic continuation from the biharmonic to the harmonic ϕ^4 model. *arXiv* **2024**, arXiv:2410.18426.
15. Cuevas-Maraver, J.; Kevrekidis, P.; Williams, F. *The Sine-Gordon Model and its Applications, Nonlinear Systems and Complexity*; Springer: Cham, Switzerland, 2014.
16. McLachlan, R. A gallery of constant-negative-curvature surfaces. *Math. Intell.* **1994**, *16*, 31–37. [CrossRef]
17. Frenkel, J.; Kontorova, T. On the theory of plastic deformation and twinning. *J. Phys. Acad. Sci. USSR* **1939**, *1*, 137.

18. Barone, A.; Paternò, G. *Physics and Applications of the Josephson Effect*; Wiley: Hoboken, NJ, USA, 1982.
19. Malomed, B.A. *The Sine-Gordon Model: General Background, Physical Motivations, Inverse Scattering, and Solitons*; Springer International Publishing: Cham, Switzerland, 2014; pp. 1–30.
20. Macías-Diaz, J.E.; Bountis, T. An efficient dissipation-preserving numerical scheme to solve a caputo–riesz time-space-fractional nonlinear wave equation. *Fractal Fract.* **2022**, *6*, 500. [CrossRef]
21. Birnir, B.; McKean, H.P.; Weinstein, A. The rigidity of sine-gordon breathers. *Commun. Pure Appl. Math.* **1994**, *47*, 1043–1051. [CrossRef]
22. Garrappa, R. Numerical solution of fractional differential equations: A survey and a software tutorial. *Mathematics* **2018**, *6*, 16. [CrossRef]
23. Bountis, T.; Cantisán, J.; Cuevas-Maraver, J.; Macías-Díaz, J.; Kevrekidis, P.G. The dissipative effect of Caputo–time-fractional derivatives and its implications for the solutions of nonlinear wave equations. *Partial. Differ. Equ. Appl. Math.* **2024**, *11*, 100807. [CrossRef]
24. Carretero-González, R.; Cisneros-Ake, L.; Decker, R.; Koutsokostas, G.; Frantzeskakis, D.; Kevrekidis, P.; Ratliff, D. Kink–antikink stripe interactions in the two-dimensional sine–gordon equation. *Commun. Nonlinear Sci. Numer. Simul.* **2022**, *109*, 106123. [CrossRef]
25. Kivshar, Y.S.; Pelinovsky, D.E.; Cretegny, T.; Peyrard, M. Internal modes of solitary waves. *Phys. Rev. Lett.* **1998**, *80*, 5032–5035. [CrossRef]
26. Campbell, D.K.; Schonfeld, J.F.; Wingate, C.A. Resonance structure in kink–anti-kink interactions in ϕ^4 theory. *Phys. D* **1983**, *9*, 1–32. [CrossRef]
27. Manton, N.S. An effective Lagrangian for solitons. *Nucl. Phys. B* **1979**, *150*, 397–412. [CrossRef]
28. Alfimov, G.; Pierantozzy, T.; Vázquez, L. Numerical study of a fractional sine-gordon equation. In *Fractional Differentiation and Its Applications*; Méhauté, A.L., Machado, J.T., Trigeassou, J., Sabatier, J., Eds.; U-Books Verlag: Augsburg, Germany, 2005.
29. Chirilus-Bruckner, M.; Kevrekidis, P.; Cuevas-Maraver, J. Stability of breathers for a periodic Klein–Gordon equation. *Entropy* **2024**, *26*, 756. [CrossRef] [PubMed]
30. Kevrekidis, P.; Carretero-González, R.; Cuevas-Maraver, J.; Frantzeskakis, D.; Caputo, J.-G.; Malomed, B. Breather stripes and radial breathers of the two-dimensional sine-gordon equation. *Commun. Nonlinear Sci. Numer. Simul.* **2021**, *94*, 105596. [CrossRef]
31. Flach, S.; Gorbach, A.V. Discrete breathers—Advances in theory and applications. *Phys. Rep.* **2008**, *467*, 1–116. [CrossRef]
32. Sulem, C.; Sulem, P. *The Nonlinear Schrödinger Equation: Self-Focusing and Wave Collapse*; Springer: New York, NY, USA, 1999.
33. Ablowitz, M.; Prinari, B.; Trubatch, A. *Discrete and Continuous Nonlinear Schrödinger Systems*; Cambridge University Press: Cambridge, UK, 2004.
34. Mainardi, F. Fractional relaxation-oscillation and fractional diffusion-wave phenomena. *Chaos Solitons Fractals* **1996**, *7*, 1461–1477. [CrossRef]